Catalysis Surveys from Asia (2018) 22:95–104
https://doi.org/10.1007/s10563-018-9242-9

Selective Catalytic Reduction of NO_x with NH_3 on Cu-BTC-derived Catalysts: Influence of Modulation and Thermal Treatment

Haoxi Jiang[1,2] · Shutian Wang[1,2] · Caixia Wang[1,2] · Yifei Chen[1,2] · Minhua Zhang[1,2]

Abstract
In this work, copper-based metal organic frameworks $Cu_3(BTC)_2$ (BTC = 1,3,5-benzenetricarboxylatle), were applied in the conversion of toxic oxynitride into nitrogen at low temperature. Scanning electron microscope (SEM), thermal gravimetric analysis (TGA), X-ray photoelectron spectroscopy (XRD) and other characterization methods were employed to fully understand the properties of the catalysts. We introduced acetic acid into the synthesis process as the modulator of the crystal structure and morphology. The catalytic assessment indicated that compared with the prototype, modified Cu-MOFs materials obtain enhanced catalytic activity for the SCR reaction. Besides, several thermolysis experiments were conducted to explain structure–function relationship.

Keywords Metal organic framework · NH_3 SCR · Morphology control · Hierarchical porous structure · Lattice defects

1 Introduction

Metal organic frameworks (MOFs), also named as porous coordination polymers (PCPs), have become known as a leading class of porous materials over the past two decades. The coordination of metal ions with multi-functional organic linkers leads to periodic structure which provides well-defined cavities for the adsorption of guest molecules, imbedding of catalytic species or immobilization of nanoclusters [1]. During the last decade, in addition to gas storage and separation [2, 3], MOFs had extended its relevance to the fields of catalytic reaction, sensing, magnetism [4], support for metal nanoparticles [1] and even toxic gas removal [5].

Since MOFs material consists of inorganic building blocks connected by organic linkers, the composite may solve the inherent problems and retain the advantages of heterogeneous catalysis [6]. Since the initial attempt which for the first time reported the application of MOFs catalyst in 1994 [7], the feasibility to utilize MOFs as catalyst or support material has been investigated for a broad range of reactions [8–10].

As a major class of atmospheric pollutant, nitrogen oxides (NO_x) have a serious impact on environment and human health. Currently, the selective catalytic reduction with NH_3 (NH_3–SCR) is the most effective and economic method for denitrification (de-NO_x). The development of low temperature de-NO_x catalyst has attracted extensive attentions in a variety of fields such as tail gas treatment, ecological improvement and the removal of toxic gas. Recently the practical applications of MOFs-derived materials towards selective catalytic reduction with NH_3 at low temperature emerged throughout the world gradually. Zhang et al. [11] synthesized binary metal organic frameworks (Fe–Mn)-MIL-100 which achieved a highest NO conversion of 96% at 260 °C and exhibited SO_2/H_2O resistance. Previously our group has reported the employment of Cu-MOF-74 which gave ideal NO conversion and near 100% N_2 selectivity at 320 °C [12].

Cu-BTC, also known as HKUST-1 or Cu-MOF-199 [13], for example, is a kind of MOFs material which has been investigated comprehensively. Usually it's synthesized by self-assemble of $Cu(NO_3)_2$ with trimesic acid (H_3BTC). Copper ions are dimerized to Cu_2 clusters which are connected coordinately with H_3BTC ligands, forming so-called

✉ Yifei Chen
yfchen@tju.edu.cn

[1] Key Laboratory for Green Chemical Technology of Ministry of Education, R&D Center for Petrochemical Technology, Tianjin University, Tianjin 300072, People's Republic of China

[2] Collaborative Innovation Center of Chemical Science and Engineering, Tianjin 300072, People's Republic of China

paddlewheel building blocks. These units connect jointly to form a 3-D porous cubic structure whose pore size allows the diffusion and adsorption of common gas molecules [14, 15]. The synthetic strategy provides not only operational ease but also the axial coordination sites pointing at the pores of the framework and weakly occupied by solvent molecules. Once the occupying molecules are removed, free coordination sites will be revealed. These unsaturated metal sites show Lewis acidity which is suitable for the activation of NH_3.

To improve the catalytic performance and extend the sphere of application, novel ideas for the modification, improvement and functionalization of MOFs material have been continuously proposed. Recently several institutes have reported the inevitable role solvent plays in the selecting of the morphological details and the matrix topology of the catalyst [16, 17]. Inspired by these works, we focused our attention on the adjustment of the ratio and species of ligands in the solvent environment by introduce ionizable conditioning agent into it, such as acetic acid.

In this study, a series of Cu-BTC-derived catalytic materials for low temperature SCR reaction were prepared. We tried to improve the catalytic performance by acidic modification. The catalytic performance of the MOFs before/after modification was compared. The results reveal that the modulation by protonic acid is an efficient route to obtain hierarchical porous Cu-MOFs derivates without structure decomposition.

2 Experimental Section

2.1 Materials

All reagents and materials were purchased commercially and used without any further treatment unless noted.

2.2 Catalyst Synthesis

$Cu_3(BTC)_2$ and derivates were prepared by a hydrothermal method according to the procedures described in other reports [18–20]. H_3BTC was dissolved in 1:1 mixture of DMF/EtOH while $Cu(NO_3)_2{\cdot}3H_2O$ was dissolved in deionized water. The solutions were combined with stirring for 10 min. Then the reaction mixture was heated at 100 °C for 10 h in an autoclave. After cooling and filtration, solid residues were washed with 1:1 mixture of EtOH/H_2O and immersed in methanol overnight. The solvent was exchanged every 12 h for 3 days. The product was preserved under vacuum and named Cu-BTC.

There was a slight change in the preparation of MOFs modulated by acetic acid. We filled three beakers with equal volume of reaction mixture, and added a certain amount of acetic acid into the solutions respectively. By the same treatments as the preparation of Cu-BTC, products with diverse degree of modulation were obtained and named 10%-AA, 20%-AA and 25%-AA as far as the approximate content of acetic acid in the solutions.

2.3 Characterization

The measurements of specific surface area were performed on a Micromeritics ASAP 2020 N_2 sorption/desorption system at 77 K. The data, including specific area and micro/mesoporous volume was calculated by BET, HK formulas and t-plot methods. TGA experiments were operated using a METTLER TGA/DSTA851 thermal gravimetric analyzer to analyze the decomposition. The flow rate was set at 20 mL/min and the heating rate was 10°C/min. Powder X-ray diffraction (XRD) patterns were acquired with the aid of a RIGAKU D/MAX 2500 diffractometer using Cu Kα radiation (40 kV, 200 mA). The morphology of the sample prepared was characterized by scanning electronic microscope (SEM) carried out by a BHK S-4800 microscope. The X-ray photoelectron spectra (XPS) was recorded with a PerkinElmer PHI-1600 X-ray spectrometer using Mg Kα radiation source and the binding energy (BE) of the C 1 s peak was set to 284.6 eV. With the combination of a Micromeritics AutoChemII 2920 adsorption instrument and a Balzers PFEIFFER-ThermoStarTM quadrupole mass spectrometer, temperature programmed desorption of NH_3 and NO was carried out to get information about the sample's surface adsorption capacity. During these experiments, the pretreated ample was exposed to 1% NH_3 (or NO) in a He mixed stream. And the desorption curves were recorded with a linear program of heating from 100 to 400 °C at the rate of 10°C/min. Fourier transform infrared (FTIR) spectra were recorded by Nicolet 6700 FTIR Spectrometer with the range from 400 to 4000 cm^{-1}.

2.4 Stability Studies

For thermal stability experiment, metal oxides derived from Cu-BTC were obtained through the thermolysis of as-synthesized MOFs materials. In the atmosphere of nitrogen or air, MOFs templates were heated in the tube furnace with a rate of 2°C/min until set temperature, and then incubated for 3 h.

For acid resistance experiment, the overall workflow is similar with a typical catalytic activity test. The adjustment is that after activation of the catalyst, we add a portion of HNO_3 solution into the reactor by a metering pump in a rate which is equal to the possible maximum generating rate of HNO_3 (all nitric oxide turn into nitric acid). The amount of water in the HNO_3 solution is equivalent to 5% feed gas.

2.5 Activity Measurements

The catalytic activities of $Cu_3(BTC)_2$ and derivates for low temperature NH_3-SCR reaction were determined by a fixed-bed reactor evaluation system. In a typical catalytic activity test, 0.2 g of sample was weighed and transferred into the reactor. Before reaction process the samples were heated with a rate of 5 °C/min until 230 °C to get activated for a duration of 3 h. Then the feed gas was flowed with a rate of 100 mL/min at room pressure to achieve a GHSV of 50,000 h^{-1}. The reaction conditions were as follows: 1000 ppm of NO, 1000 ppm of NH_3, 2% of O_2 and argon as balance gas.

The gas-phase concentrations of NO_x were monitored by a Kane KM9106 flue gas analyzer and the composition was monitored by an Agilent 6820 gas chromatograph. The NO conversion was obtained from the inlet and outlet NO concentrations at each temperature started from 80 °C while the selectivity was obtained from the compostion of the outlet ananlyzed by gas chromatograph. NO conversion and N_2 selectivity were calculated by the following equations:

$$\text{No conversion} = \frac{[NO]_{inlet} - [NO]_{outlet}}{[NO]_{inlet}} \times 100\%$$

$$N_2 \text{ selectivity} = \frac{[N_2]}{[N_2] + [N_2O]} \times 100\%.$$

3 Results and Discussion

3.1 Catalytic Performance

Based on the results of assessment shown in Fig. 1, it can be deduced the employment of acetic acid leads to a marked increase in catalytic performance, especially at low temperature. With the addition of modulator, the catalytic activity of Cu-BTC is enhanced and reaches the highest productivity at the 25%-AA sample, which is 95.5% at 280 °C. Through the whole temperature range, no occurrence of N_2O has been detected and the selectivity of N_2 is close to 100%.

3.2 Characterization of Cu-BTC and Modulated Derivates

Nitrogen adsorption–desorption isotherms of Cu-BTC sample are shown in Fig. 2a. Apparently we have got a type I isotherm which indicates that pore sizes mainly distribute in microporous magnitude (about 2 nm on average). The rapid increase of adsorption in the log plot shows

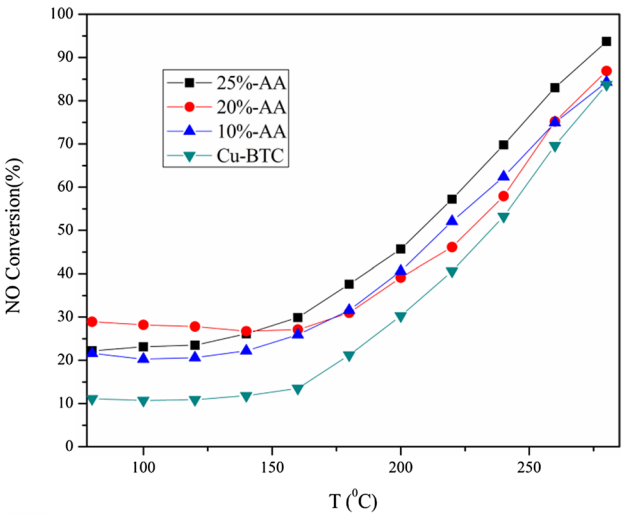

Fig. 1 The SCR activities of Cu-BTC and derivates modulated by acetic acid

that the Cu-MOFs material has concentrated pore diameter distribution. The MOFs sample has a BET specific area of 1439.7 m^2/g and a pore volume of 0.629 cm^3/g.

The powder X-ray diffraction pattern of Cu-BTC sample is shown in Fig. 2b. A pattern calculated from crystallographic data is also provided to compare. By comparison the overall agreement is good and a couple of characteristic diffraction peaks are obvious ($2\theta = 6.6°$ for (200), 9.5° for (220), 11.6° for (222), 13.4° for (400), 17.4° for (333), 19.0° for (440) crystal plane). There are some deviations between two patterns due to structure defects and coordinated solvent molecules brought by synthetic process.

Figure 3(a) shows the detailed information of internal pores obtained from N_2 adsorption–desorption isotherms at low temperature. We found that the concentrated pore size distribution maintained after the modification. The textual properties of Cu-BTC and derivatives are summarized in Table 1. According to the table, with the addition of modulator, BET specific area and pore volume of copper MOFs tended to increase and reached maximums for 25%-AA sample which were 1750.0 m^2/g and 0.745 cm^3/g respectively. There were some fluctuations in the proportions of micro/mesopore volume with the increase of modulator usage. A possible explanation is that 10%-AA and 20%-AA didn't get enough drying so that a certain proportion of mesopores were blocked by solvent molecules.

The powder X-ray diffraction patterns of the original Cu-MOFs and derivates are summarized in Fig. 3b. In order to facilitate comparison, all curves have been normalized as far as the intensity of the strongest peak, which is (222) peak. Hence when comparing (222) peak, we should focus on the relative strength of the diffraction peak to the other ones. Undoubtedly they share the same crystal structure in

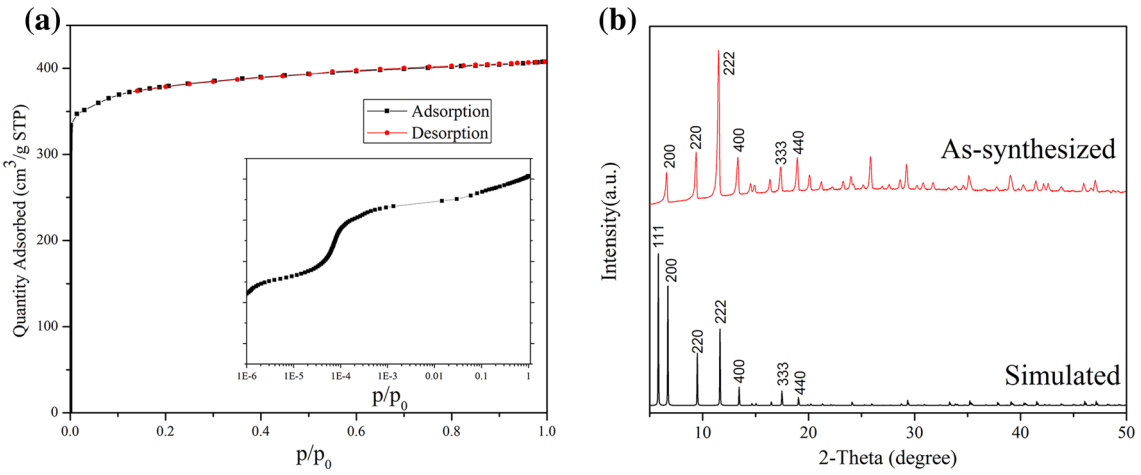

Fig. 2 **a** The N_2 adsorption–desorption isotherms, **b** XRD pattern of Cu-BTC

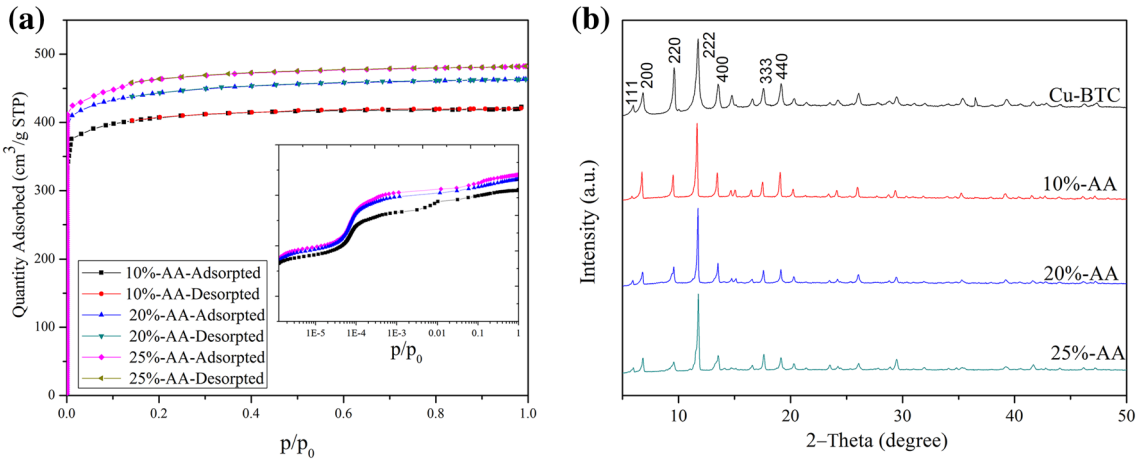

Fig. 3 **a** The N_2 adsorption–desorption isotherms and **b** XRD patterns of derivates modulated by acetic acid

Table 1 The textural properties of Cu-BTC and derivates

Samples	BET specific area (m^2/g)	Pore volume (cm^3/g)	Average diameter (Å)
Cu-BTC	1439.7	0.629	17.5
10%-AA	1338.7	0.649	19.4
20%-AA	1234.6	0.650	20.0
25%-AA	1361.1	0.710	21.0

consideration that the characteristic peaks of modulated materials are in accord with those of original Cu-BTC. The (111) reflection ($2\theta = 6.6°$) is noteworthy because the intensity of it is associated with the unsaturated sites. Once the H_2O molecules are removed, the crystal plane in this direction is exposed. In our work all samples were dried naturally except for original Cu-BTC sample, which was dried under vacuum. Hence among four patterns Cu-BTC sample has the intensified (111) reflection. By closer inspection on the other patterns, we found that the intensity of (111) peak reinforces with the increase of acetic acid content. The phenomenon is probably attributed to the role of template agent acetic acid plays in the reaction [21–23]. The (111) plane was preferentially occupied by acetic acid molecules during the synthetic process. Since acetic acid is easy to be replaced by agents like methanol or ethanol, the intensified (111) reflection after extraction indicates that unsaturated sites are exposed completely with the addition of acetic acid. It can also be concluded that the crystallinity of the framework decreases and that lattice constants change in view of the phenomenon that most peaks weakened after the addition of modulator and that the position of all peaks shifted to lower 2θ angle.

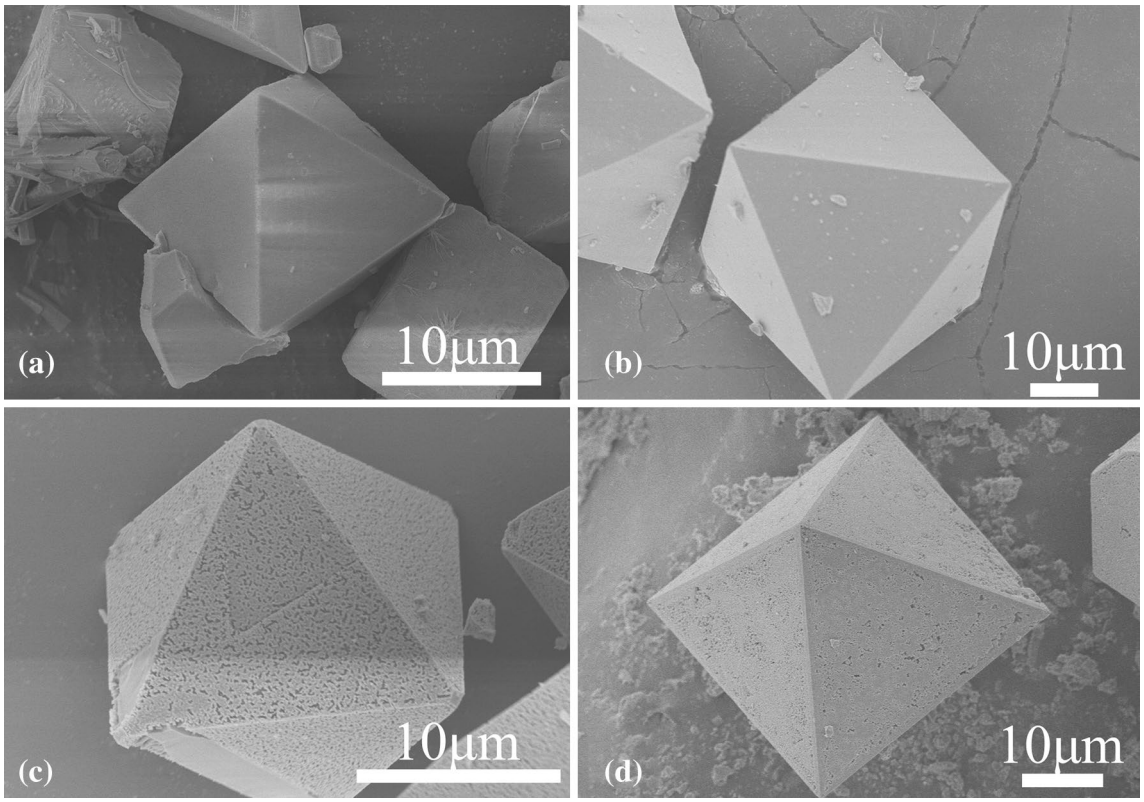

Fig. 4 SEM micrographs of Cu-BTC and derivates modulated by acetic acid **a** Cu-BTC, **b** 10%-AA, **c** 20%-AA, **d** 25%-AA

Scanning electron microscope micrograph was carried out to investigate the morphology of MOFs and the images are shown in Fig. 4. As-synthesized Cu-BTC (Fig. 4a) exhibits regular octahedron crystal form which is in good agreement with the literature report [14, 18]. The size of the particles in captured images ranges from 10 to 30 μm. When enough acetic acid was employed, irregular microporous to mesoporous structures at the surface appeared while the edges and corners of lattice cell sharpened. The phenomenon is related to the preferred growth of (222) plane. In addition, a closer observation revealed a trend toward surface roughening with modulator adding. The tendency is in good agreement with the results of XRD in that the modulator introduces defects into the crystal and the morphology with comprehensive hierarchical porous structure form.

All the results can be explained by the following ways. As organic acid, firstly, acetic acid competes with H_3BTC to occupy coordination sites. Such competitive behaviors lower the complex formability of the framework and retard crystal growth. Secondly a small quantity of acetic acid molecules ionize in the solvent environment and hinder the deprotonation of the organic linkers. Thirdly as capping agent, acetic acid shows selective retardation to crystal growth of specific direction. Lastly during assemble process, some acetic acid molecules act as linkers, but due to their instability, these so-called "framework fragments" give rise to the formation of defects in the crystal. As a whole, these effects on assemble synergistically lead to lattice imperfection and the decrease of crystallinity.

Through temperature programmed desorption experiments, we get the information about the adsorption behaviors towards specific molecules and the acidity on the surface of the catalyst surface under reaction conditions. In the NH_3-TPD curve (Fig. 5a), we find a desorption peak located at around 173 °C, which suggests the exclusive presence of weak acid sites scattering on the surface and a desorption peak located at around 337 °C which is caused by self-decomposition. The NO-TPD curve (Fig. 5b) indicates that the material exhibits little specific adsorption towards NO since there is no obvious desorption peak except for the one associated with skeleton decomposition. Thus the reaction processing on the material surface follows the E–R mechanism.

The valence states of as-synthesized Cu-BTC were also investigated by X-ray photoelectron spectroscopy. As shown in Fig. 5c, only one O1s characteristic peak located at 531.7 eV is observed, suggesting that the coordination between carboxyl oxygen and metal nodes is stable, and under the condition of XPS test, water or other solvent molecules have been already removed from copper sites.

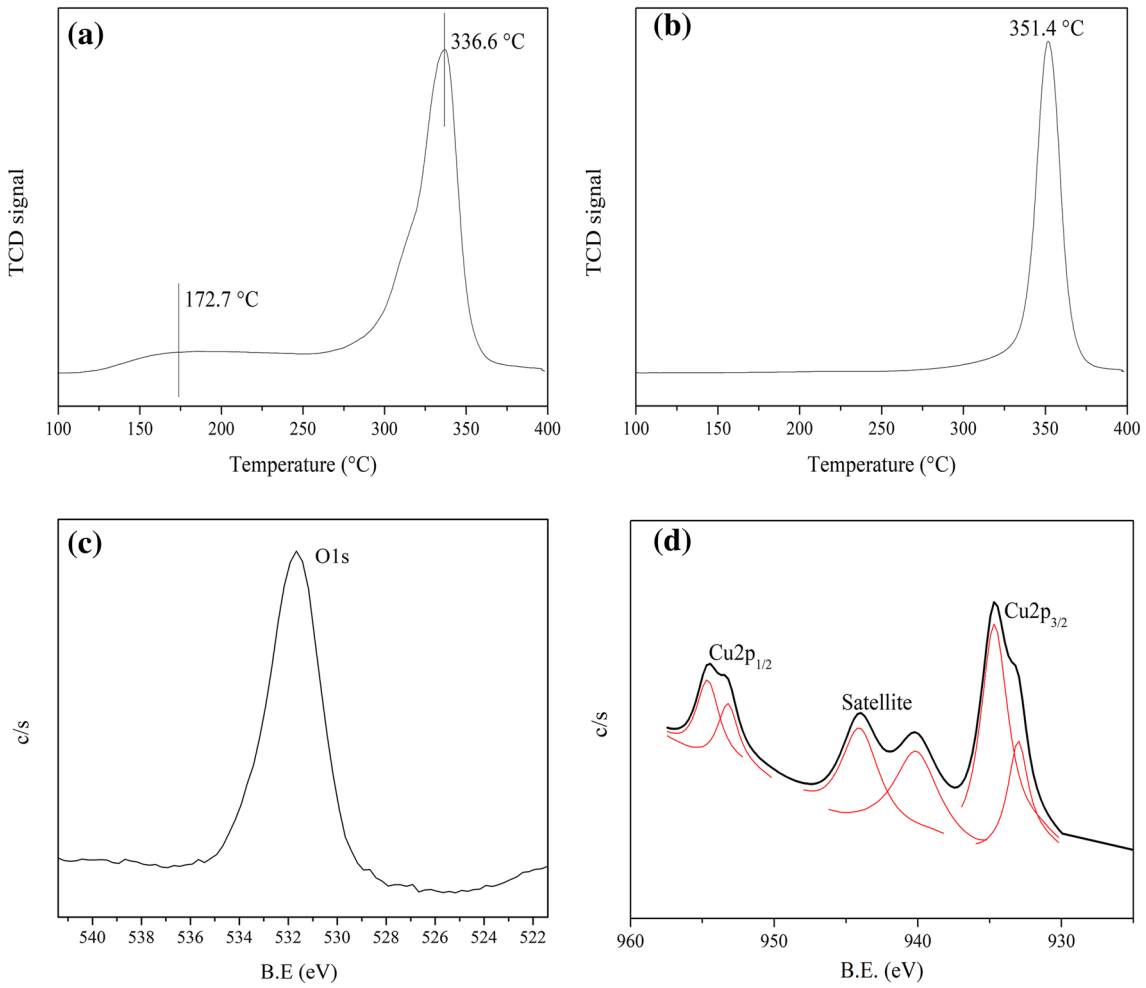

Fig. 5 Temperature programmed desorption curves with **a** NH_3 and **b** NO as probe molecules and **c** and **d** XPS spectra of Cu-BTC

Figure 5d shows a partially enlarged view of Cu2p spectrum and the peak fitting results of copper species spectrums are attached to it. The obvious satellite peaks located around 940 eV indicate the appearance of Cu^{2+} ions and the disproportionation of every characteristic peak confirms the coexistence of Cu^{2+} and Cu^{+} species on the surface [24]. The information XPS measurements provide is summarized in Table 1, together with the XPS characteristic peaks of copper oxides. The gaps of binding energy between the surface species of MOFs and oxides reflect the reinforcement on the electron cloud density brought by coordination interaction [25].

In order to further determine the structure of the composite, we have made the FTIR characterization of the sample, as shown in Fig. 6. The absorption peak at 3430 cm^{-1} is ascribed to the stretching vibration of adsorbent water molecules, and this peak proves that solvent molecules such as water and methanol still exist on the surface of MOFs materials. The telescopic vibration peak at 1584 cm^{-1} is derived from the water molecules coordinated with metal nodes. The absorption peaks of 1640, 1450 and 1375 cm^{-1} are associated with the stretching vibration (both symmetric and asymmetric) of carboxylate radical. The absorption peaks at 874, 759 and 728 cm^{-1} in the fingerprint area show obvious benzene ring characteristics. All of the above information shows that the organic metal structure of the composite is consistent with Cu- BTC [26]. In the atlas of modified products, all Cu-BTC characteristic peaks are present, which prove that the modification of acetic acid has little effect on the organic composition of MOFs material (Table 2).

In SCR atmosphere, NO_x could be transferred into HNO_3 in the presence of moisture, which may cause damage to the MOFs structures. To examine the tolerance to harsh acid environment, a stability assessment experiment was carried out. After 12-h HNO_3 treatment, the XRD pattern of the catalysts recycled was compared with freshly prepared ones (Fig. 7). It's obvious that through acid treatment possible occurs in low temperature SCR reaction system, the crystal structure of MOFs didn't break.

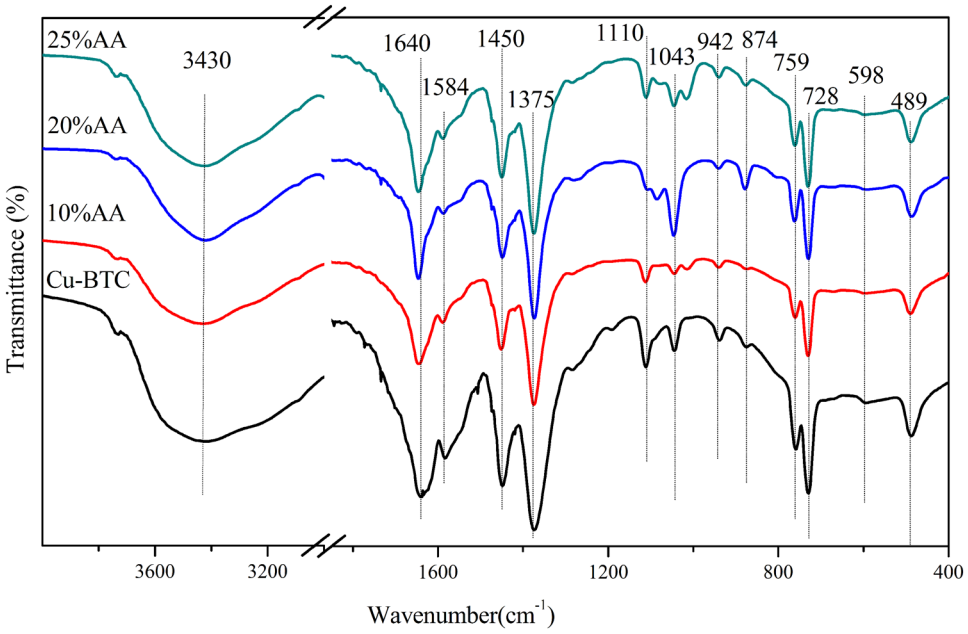

Fig. 6 FTIR spectra of Cu-BTC and derivates modulated by acetic acid

Table 2 States and element composition of Cu species on the surface of Cu-BTC

Species	BE 2p3/2 (eV)	Satellite (eV)		BE 2p1/2 (eV)
Cu^{2+}	934.7	940.1	944.1	954.6
Cu^{+}	933.0	–	–	953.2
CuO	993.8	939.0	944.0	953.8
Cu_2O	932.8	–	–	952.8

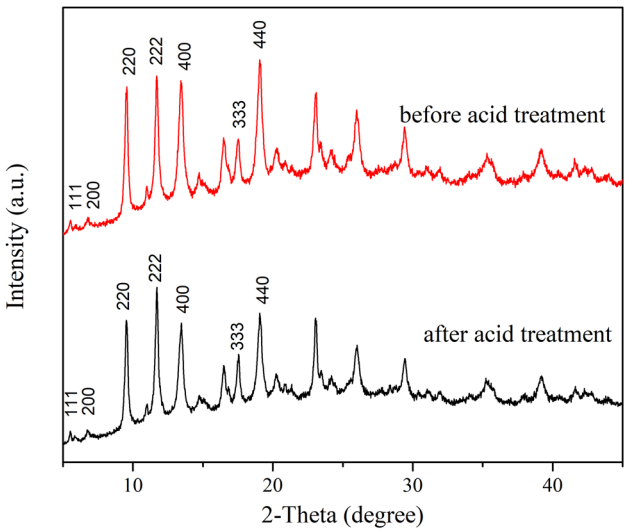

Fig. 7 XRD patterns of Cu-BTC samples before/after acid treatment

To examine the effects on the thermal stabilities by modulation, thermal gravity analysis was operated to every as-synthesized sample and the curves are shown in Fig. 8. From the results it can be observed that under every atmosphere, there's a tiny gap in thermal stability between 25%-AA and other samples which caused by low crystallinity and lattice defects.

In summary, compared with original catalyst, the most obvious changes for modified products in structure and morphology are the appearance of mesoporous structure, slight crystal form transition and lattice defects. However, in the low temperature SCR reaction system, without sintering and blockage of the catalyst, the influence of diffusion is very small for the reaction process, which is to say, the change of pore structure is not the main factor of the activity enhancement. So it's likely that certain degree of lattice defects and the sharpening of specific (111) crystal plane give rise to the improvement of catalytic performance. To find out the dominating factor of catalytic activity, we then conducted a series of thermal decomposition experiments to Cu-BTC sample. And these experiments gave an interesting reason of activity reinforcement.

3.3 Thermal Stability Assessment and Thermal Decomposition of Cu-BTC

It's widely known that MOFs material can be transferred into metal oxide catalysts by direct pyrolysis. And the strategy that MOFs are used as the precursors or templates for the synthesis of derived catalysts by pyrolysis provides a way to design functional material with specific crystal structure [27–29]. On the other hand, however, in some cases

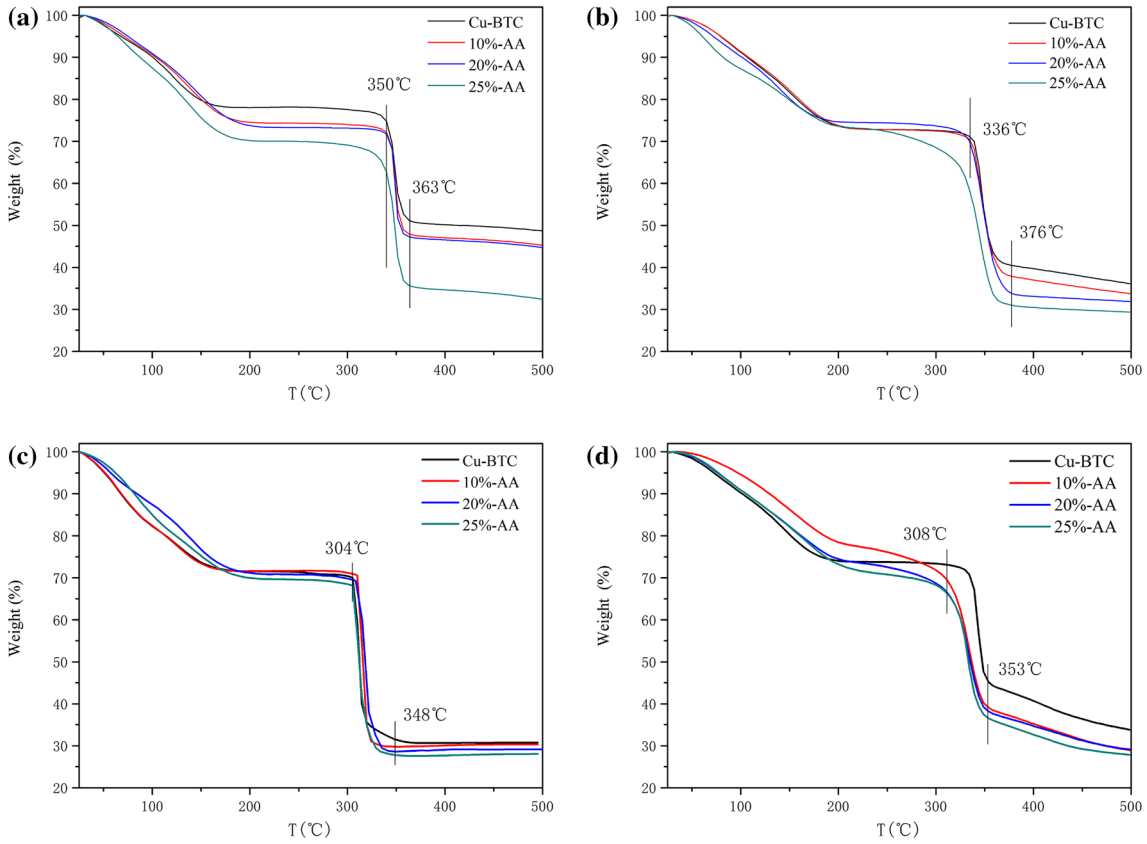

Fig. 8 The TG curves of Cu-BTC and derivates modulated by acetic acid under different atmospheres: **a** N_2, **b** 2% H_2/N_2, **c** Air and **d** the SCR reaction gases

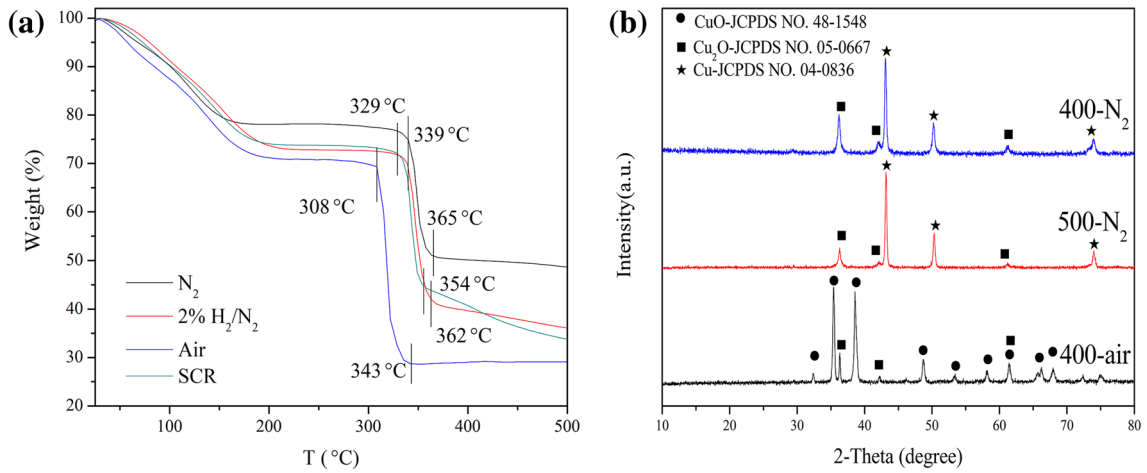

Fig. 9 **a** The TG curves of Cu-BTC under different atmospheres and **b** XRD patterns of derivates obtained by the thermolysis of Cu-BTC

of MOFs application, overheating to decomposition cannot retain the morphology and characteristics of MOFs catalyst and will impair the catalytic activity. Hence we tried to figure out the effect on the catalyst performance by pyrolysis. Firstly we studied the thermal stabilities of Cu-BTC with various atmospheres (N_2, 2% H_2/N_2, air and the SCR reaction gases) using TGA and the curves are shown in Fig. 9a. The first weight loss terminated at about 100 °C is ascribed to the evaporation of solvent molecules. The sample maintained stability in framework when the temperature was

under 300 °C. After further heating, the organic linkers were completely stripped till 380 °C at which MOFs material ultimately turned to copper. Based on the curves of thermal stability characterization, we chose N_2 as the pyrolysis atmosphere and the heating temperature was set to 400 °C. As contrast, products pyrolyzed under air at 400 °C and N_2 at 500 °C were also prepared.

The XRD patterns of thermally decomposed MOFs are shown in Fig. 9b. For Cu-BTC samples heated in N_2, they turned to mixtures of cuprite (JCPDS NO. 05-0667) and copper (JCPDS NO. 04-0836) after thermolysis, either at 400 or 500 °C. A milder and inert environment was provided for those samples in the atmosphere of nitrogen so that skeleton-derived carbon played the role of reductant and we got copper oxides with lower valence. The sample heated at 400 °C in air is the mixture of tenorite CuO (JCPDS NO. 48-1548) and cuprite Cu_2O.

To get a comprehensive understanding to the structure–activity relationship, we weighed a certain amount of every sample and evaluated their activities with the procedure described before (Fig. 10). Among three samples with thermal treatment, the sample heated in N_2 at 400 °C exhibits the best catalytic performance which gives a NO conversion of 83.9% at 280 °C. We were confused by the figure since the catalytic activity of Cu-BTC is not as good as two heated samples throughout the temperature range, except for the last point. Besides, by comparison of three samples, it's obvious that the heating temperature dominates activity rather than the choice of atmosphere which has a great impact on the morphology. Based on the work in previous sections and the comparison in performance, we figured that the loss of organic ligands induced by temperature increase is crucial in performance. For a mild temperature which slightly excesses the temperature limit of MOFs (like 400 °C), though the coordinate bonds are broken, organic linkers are not consumed during the heating process. A possibility is that inspired by inadequate heat energy, these ligands tend to externalize to the surface of the crystal particle, thus reinforce the surface acidity and the activation of ammonia molecule coincidently. And for the same reason, the catalyst seems to be "more active" after heating at 400 °C. As the reaction progresses, superficial carboxyl and hydroxyl groups will be removed with the gas flow and heated MOFs lose its activity gradually. The deduction is proved by the fact that after hours of experiment, the activity of Cu-BTC ultimately exceeded the heated samples at 280 °C. It can also be concluded that in low temperature NH_3-SCR reaction catalyzed by porous compounds, diffusion and contact of reactants have little effect on the conversion.

To prove our assumption, it's necessary to get detailed information related to the organic groups. As a result, all samples prepared were characterized by Fourier transform infrared spectrometry. As shown in Fig. 11, the patterns are all normalized as far as the maximum of absorbance, so the intensity of every peak has a positive relationship with the accurate density of corresponding functional groups. Intuitively peaks related to the hydroxyl and carboxyl marked in Fig. 11 confirmed the hypothesis in that the intensities of key peaks in Cu-BTC pattern are much higher than those in heated samples. (The peak located at 1640 cm^{-1} is ascribed to the anti-telescopic vibration of carboxylate radical which happens to overlap the bending vibration bands of adsorbed H_2O, so the measurement in this peak is invalid.) In addition, by contrasting data it can be discriminated easily that samples heated at higher temperature have lower response to organic group detection.

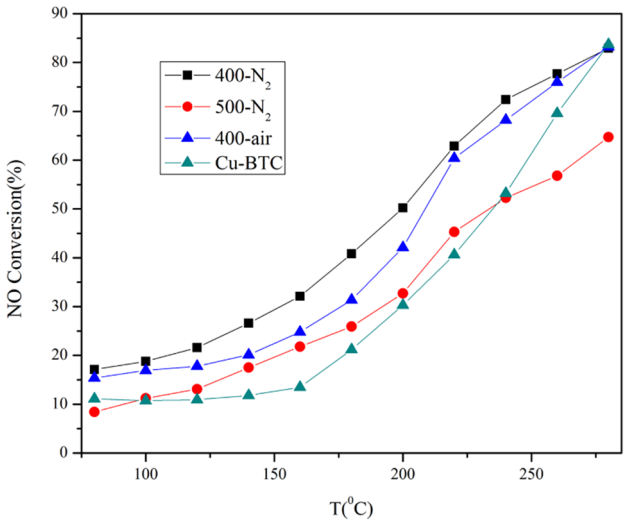

Fig. 10 The SCR activities of Cu-BTC and metal oxides obtained by the thermolysis of Cu-BTC

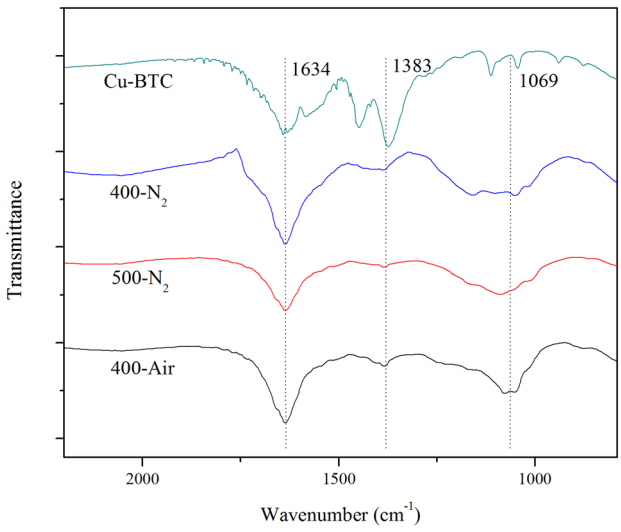

Fig. 11 FTIR spectra of derivates obtained by the thermolysis of Cu-BTC

To sum up, in this section, we compare possible reasons for the deactivation of catalyst and the most influential factor of them is very likely to be the distribution of these functional organic groups, rather than copper species valence, crystal form and surface area. But still we can't rule out the possibility that lattice defects benefit the reaction progress.

4 Conclusions

In summary, Cu-MOFs catalysts and derivates modified by acetic acid were successfully prepared by a conventional solvothermal method in this work. By the employment of modulator, a hierarchical porous structure with beneficial lattice imperfection is achieved. The results of heating experiments demonstrate that during the process, temperature weighs more in the determination of activation because the heat-sensitive organic ligands mainly influence the active sites on the surface. Acid-modulated Cu-BTC derivates give better catalytic performances with the highest NO conversion of 95.5% at 280 °C. The overall conclusion of this preliminary work is that as-synthesized MOFs material has great development potentiality for low temperature NH_3-SCR reaction.

Acknowledgements This work was supported by National Natural Science Foundation of China (Nos. 21506150, 21406159) and also by the Scientific Research Foundation for the Returned Overseas Chinese Scholars, State Education Ministry.

Compliance with Ethical Standards

Conflict of interest The authors declares that they have no conflict of interest.

References

1. Müller M, Hermes S, Kähler K, Berg MWEVD, Muhler M, Fischer RA (2008) Chem Mater 20:4576
2. Xiao B, Paul W, Zhao X (2007) J Am Chem Soc 129:1203
3. Yaghi OM, Li G, Li H (1995) Nature 378:703
4. Herbst A, Khutia A, Janiak C (2014) Inorg Chem 53:7319
5. Montoro C, Linares F, Procopio EQ, Senkovska I, Kaskel S, Galli S, Masciocchi N, Barea E, Navarro JA (2011) J Am Chem Soc 133:11888
6. García P, Müller M, Corma A (2014) Chem Sci 5:2979
7. Fujita M, Kwon YJ, Washizu S, Ogura K (1994) J Am Chem Soc 116:1151
8. Hermes S, Schröter MK, Schmid R, Khodeir L, Muhler M, Tissler A, Fischer RW, Fischer RA (2005) Angew Chem Int Ed 44:6237
9. Ingleson MJ, Barrio JP, Guilbaud JB, Khimyak YZ, Rosseinsky MJ (2008) Catal Commun 23:2680
10. Gascon J, Aktay U, Hernandez-Alonso MD, Klink GPMV., Kapteijn F (2009) J Catal 261:75
11. Zhang W, Shi Y, Li C, Zhao Q, Li X (2016) Catal Lett 146:1956
12. Jiang HX, Zhou JL, Wang CX, Li YH, Chen YF, Zhang MH (2017) Ind Eng Chem Res 56:3542
13. Chui SS, Lo SM, Charmant JP, Orpen AG, Williams ID (1999) Science 283:1148
14. Kim J, Cho HY, Ahn WS (2012) Catal Surv Asia 16:106
15. Wang QM, Shen D, Bülow M, Lau ML, Deng S, Fitch FR, Lemcoff NO, Semanscin J (2002) Microporous Mesoporous Mater 55:217
16. Huang WH, Yang GP, Chen J, Chen X, Zhang CP, Wang YY, Shi QZ (2012) Cryst Growth Des 13:66
17. Jia MC, Chen EY, Menon AG, Tan HY, Hor ATS, Schreyer MK, Xu J (2012) Crystengcomm 15:654
18. Chowdhury P, Bikkina C, Meister D, Dreisbach F, Gumma S (2009) Microporous Mesoporous Mater 117:406
19. Jinchen L, Culp JT, Sittichai N, Bockrath BC, Brian Z, Giovanni G, Karl J (2007) J Phys Chem C 111:9305
20. Rowsell JL, Yaghi OM (2006) J Am Chem Soc 128:1304
21. Stock N, Biswas S (2012) ChemInform 43:933
22. Yang H, Orefuwa S, Goudy A (2011) Microporous Mesoporous Mater 143:37
23. Schaate A, Roy P, Godt A, Lippke J, Waltz F, Wiebcke M, Behrens P (2011) Chem Eur J 17:6643
24. Chen LF, Guo PJ, Qiao MH, Yan SR, Li HX, Shen W, Xu HL, Fan KN (2008) J Catal 257:172
25. Tseng IH, Wu JCS, Chou HY (2004) J Catal 221:432
26. Decoste JB, Peterson GW, Schindler BJ, Killops KL, Browe MA, Mahle JJ (2013) J Mater Chem A 1:11922
27. Chen L, Zhao C, Wei Z, Wang S, Gu Y (2011) Mater Lett 65:446
28. Das R, Pachfule P, Banerjee R, Poddar P (2012) Nanoscale 4:591
29. Zhang S, Liu H, Sun C, Liu P, Li L, Yang Z, Feng X, Huo F, Lu X (2015) J Mater Chem A 3:5294